Available online at www.sciencedirect.com
ScienceDirect
Journal of Nuclear Materials 359 (2006) 139–149
journal of nuclear materials
www.elsevier.com/locate/jnucmat

A two-zone method with an enhanced accuracy for a numerical solution of the diffusion equation

Jin-Sik Cheon *, Yang-Hyun Koo, Byung-Ho Lee, Je-Yong Oh, Dong-Seong Sohn

Korea Atomic Energy Research Institute, P.O. Box 105, Yuseong, Daejeon 305-600, Republic of Korea

Received 23 May 2006; accepted 14 August 2006

Abstract

A variational principle is applied to the diffusion equation to numerically obtain the fission gas release from a spherical grain. The two-zone method, originally proposed by Matthews and Wood, is modified to overcome its insufficient accuracy for a low release. The results of the variational approaches are examined by observing the gas concentration along the grain radius. At the early stage, the concentration near the grain boundary is higher than that at the inner points of the grain in the cases of the two-zone method as well as the finite element analysis with the number of the elements at as many as 10. The accuracy of the two-zone method is considerably enhanced by relocating the nodal points of the two zones. The trial functions are derived as a function of the released fraction. During the calculations, the number of degrees of freedom needs to be reduced to guarantee physically admissible concentration profiles. Numerical verifications are performed extensively. By taking a computational time comparable to the algorithm by Forsberg and Massih, the present method provides a solution with reasonable accuracy in the whole range of the released fraction.

PACS: 28.41.Ak; 66.30.−h

1. Introduction

A distinctive feature in a fuel performance code relative to others is the consideration of a fission gas release during reactor operation [1]. Numerous models have been developed to understand the fission gas release (FGR) where the flux of gas atoms to the grain boundaries is described by a diffusion equation together with proper boundary conditions. The solutions of the equation are sought analytically as well as numerically [2–6]. Among the numerical treatments, the variational principle applied to the equation is regarded as one of the most suitable methods in the sense of an accuracy and efficiency. A finite element (FE) analysis is this kind of method. The accuracy of the FE analysis depends principally on how many meshes are employed and how well the trial functions represent the profile of the gas concentration.

Since a great number of solving the diffusion equation is required during a fuel performance analysis, the calculation speed is increased by impairing the accuracy of the solution with a fewer

* Corresponding author. Tel.: +82 42 868 2648; fax: +82 42 864 1089.
E-mail address: jscheon@kaeri.re.kr (J.-S. Cheon).

0022-3115/$ - see front matter © 2006 Elsevier B.V. All rights reserved.
doi:10.1016/j.jnucmat.2006.08.016

number of meshes. The two-zone method proposed by Matthews and Wood [4], follows a similar approach. Although the two-zone method requires three degree of freedoms (DOF) with two quadratic elements for a whole spherical grain which is divided into two concentric regions, it was reported to have a lower accuracy for a low release of less than 2%. The FGR of 1–2%, however, is the most important value around which a significant fission gas begins to release through open pathways formed due to the saturation process of the grain boundaries [7].

As the fission gas atoms are not diffused out to the grain boundary at an early stage of FGR, there is a steep gradient in the gas concentration near the grain surface. Such an abrupt change is described more reasonably by refining the meshes near the surface [8–11]. Furthermore, a more accurate solution can be obtained with the same number of meshes by introducing a mesh adaptivity which is explained by employing a suitable re-meshing technique through relocating the finite element (FE) nodes [12]. The mesh adaptivity is known to be effective in describing the steep gradient of a solution in a problem domain, for example, for a wetting of open porous materials [13]. Another important issue in the numerical solution of the transient diffusion equation is the interconnection of the spatial mesh size and the time step. An inappropriately small time step may result in a physically non-meaningful and spurious oscillation.

In this paper, the two-zone approaches are further extended to provide accuracy comparable to that of the FEM with very fine meshes at an early stage as well as at a higher release. This is accomplished not only by introducing the strategy of moving the interface between the two concentric regions which corresponds to the mesh adaptivity, but also by decreasing the number of the DOF for the problem.

2. Solution methods for the fission gas release

The diffusion equation in spherical coordinates,

$$\frac{\partial c_g}{\partial t} = \frac{1}{r^2}\frac{\partial}{\partial r}\left(D_{\text{eff}} r^2 \frac{\partial c_g}{\partial r}\right) + \beta \tag{1}$$

is solved with the boundary conditions, $c_g = 0$ at $r = a$ and $\partial c_g/\partial r = 0$ at $r = 0$, where a is the grain radius, D_{eff} the effective diffusion coefficient of a gas atom, and β the number of gas atoms produced per fission event.

2.1. Analytical solutions

For a zero initial condition and a constant gas generation rate, the exact solution of Eq. (1) is given by [14]

$$c_{\text{gn}} = 1 - \rho^2 + \frac{12}{\pi^3 \rho}\sum_{n=1}^{\infty}\frac{(-1)^n}{n^3} e^{-n^2\pi^2\tau}\sin n\pi\rho, \tag{2}$$

where c_{gn} is the normalized gas concentration which is defined by $6D_{\text{eff}}c_g/\beta a^2$, the normalized time $\tau = D_{\text{eff}}t/a^2$, and the normalized radial coordinate $\rho = r/a$.

Using Eq. (2), the fractional release can be obtained by

$$f(\tau) = 1 - \frac{1}{15\tau}\left\{1 - \frac{90}{\pi^4}\sum_{n=1}^{\infty}\frac{\exp(-n^2\pi^2\tau)}{n^4}\right\}. \tag{3}$$

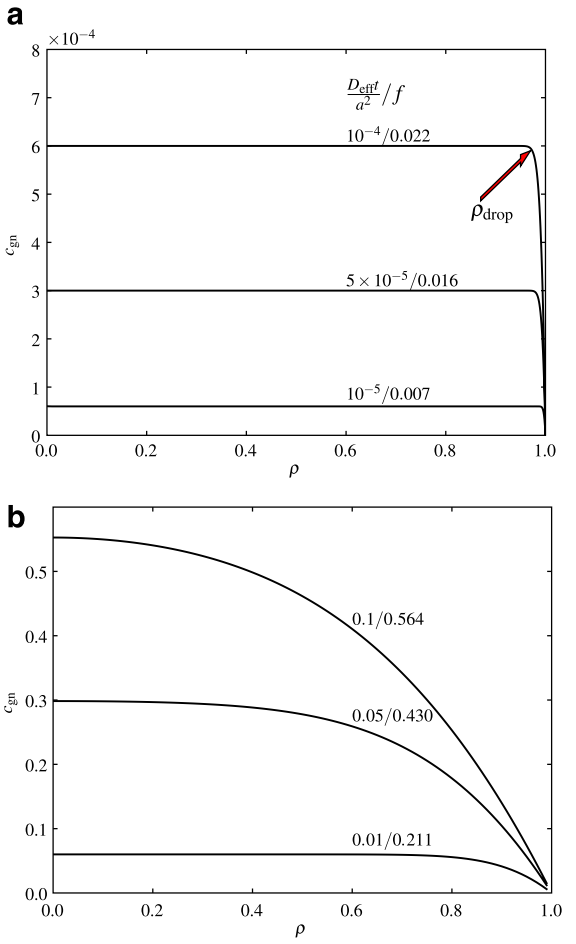

Fig. 1. Normalized gas concentration along the normalized coordinate from the exact solution for a zero initial condition and constant gas generation rate. (a) Early stage and (b) later stage.

Fig. 1 shows the distribution of c_{gn} along ρ which is calculated from Eq. (2). In this figures, the normalized time and the corresponding released fraction are noted. At an early stage, the distribution of c_{gn} is nearly flat in most of the grain. It also exhibits an abrupt drop near the surface, whose coordinate moves inward in proportion to the released fraction. The maximal concentration is always located at the center of the grain. Later, the distribution of the gas concentration can be described well by the quadratic function.

In the case of a time-varying gas generation, the fractional release is obtained by using a quasi-exact solution [5] which is used in the ANS-5.4 algorithm [3].

2.2. Numerical solutions using a variational method

An attempt to apply the variational principle to the problem of a fission gas release was made by Matthews and Wood [4]. The spherical grain is divided into two concentric regions of almost an equal volume, which are designated as region I and II, respectively. Three nodal points are required; the midpoint radius of region I ($\rho_1 = 0.4$), the interface between the regions ($\rho_2 = 0.8$), and the midpoint radius of region II ($\rho_3 = 0.9$). The concentrations at these points are represented by c_1, c_2, and c_3, respectively. Quadratic functions are employed to represent the concentration profile.

The accuracy of such a variational method with fixed nodal positions is examined in more detail. With increasing the number of the concentric regions, i.e., the number of quadratic FE, the fractional release is calculated for a reference problem as shown in Fig. 2 [15]. A commercial finite element code, ABAQUS [16] is used for this purpose.

The gas concentration and the fractional release are calculated for the three cases as follows:

(a) The number of FE is 10, and the ratio of the element length between the neighbors is 1.1.
(b) The number of FE is 10, and the grain is divided into two layers whose interface is located at an order of magnitude of the resolution depth λ from the grain surface. The inner and outer layers have 9 and 1 quadratic elements, respectively. The ratio of the element length is 1.1 and 1.0 for the two layers.
(c) All the conditions except for the number of FE are the same as those of Case (b). It is increased up to 50 which are distributed as 40 and 10 for the two layers. The number of FE and the distribution are the same as those used in the previous work [8] to obtain 'numerically exact' solutions.

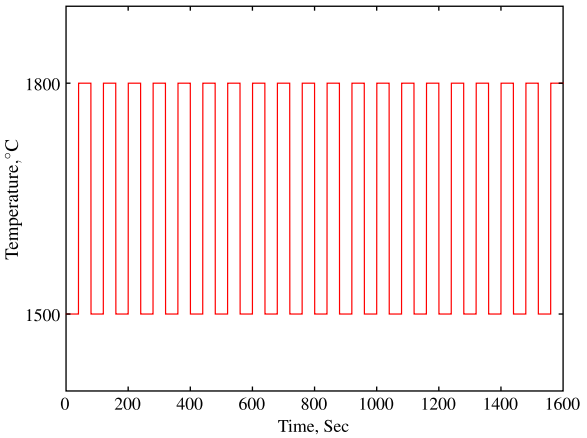

Fig. 2. Variation of temperature for a reference problem [15].

Fig. 3 shows the released fraction as a function of the time. The released fraction at the early stage is inaccurately estimated even if the number of the FE is increased by as many as 10 which are even higher than those employed in the literature [4,9]. Meanwhile, Rest [11] modified the two-zone method by locating ρ_2 at λ to represent a more accurate concentration gradient near the surface. However, it resulted in an unacceptable response for the temperature history of Fig. 2 [17].

The investigation of a gas concentration profile makes it possible to find out why the numerical methods with a limited number of the elements

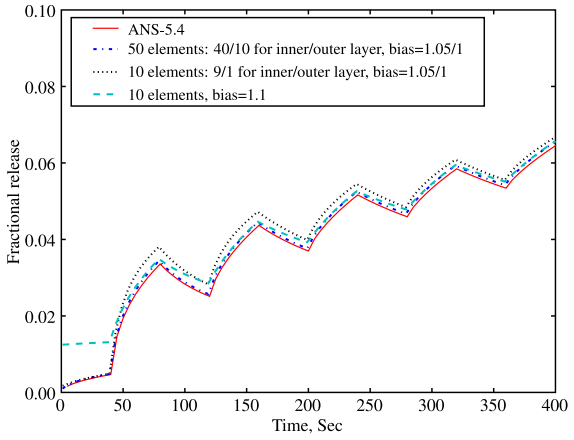

Fig. 3. Fractional release from finite element analysis with fixed nodal positions.

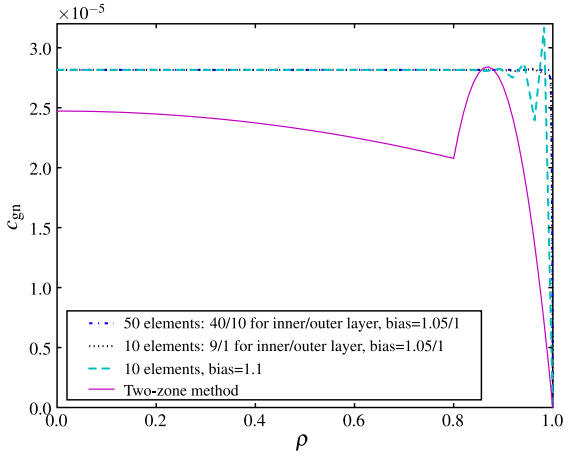

Fig. 4. Gas concentration along normalized radius from numerical methods with fixed nodal positions.

having a fixed nodal positions exhibit inaccuracies at an early stage. The gas concentration is plotted in Fig. 4 at the time of 40 s in the temperature history of Fig. 2. It is fluctuating near a grain surface, especially very seriously if an outer layer is not included in the FE model. Fig. 4 also shows the result from the two-zone method where the maximum of the gas concentration is present near the surface. In comparison, no fluctuations appear and the maximum is located at the center of the grain as in the exact solution shown in Fig. 1, when the number of FE is increased to 50.

It was reported that the same phenomena were present in the numerical solution of the transient heat equation to which the conventional Galerkin FEM was applied [18]. Here wiggles are generated near the boundary at an early time since the number of FE and the distribution are inappropriate to represent the temperature of a problem domain, especially near its surface. The spurious oscillation is more pronounced when using quadratic elements. In this regard, commercial FE codes recommend that a time increment be larger than the minimum usable one which depends on the element size and material properties [16]. For a FGR problem where a few quadratic elements are used to solve the diffusion equation, it is very likely that such fluctuations are inevitable in the vicinity of the surface when a rapid change of the temperature occurs.

3. Adaptive two-zone method

The two-zone approximation is modified to assure an enhanced accuracy while maintaining its efficiency as much as possible. Two strategies are implemented. Firstly the coordinates of the three nodal points are not fixed. Instead, they are changed in proportion to the released fraction. Secondly the number of DOF needs to be reduced so that the distribution of the gas concentration is always physically admissible.

3.1. Moving nodal points and trial functions

The movement of the nodal points is implemented by controlling the interface between the two-zones to obtain a more accurate distribution of the gas concentration near the surface. In Fig. 1(a), the profile of the gas concentration in a grain can be divided into two parts; the flat one and the other having the steep gradient. If ρ_2 is set to be located around the boundary of the two parts at every moment, it is possible that the gas concentration for both parts is described by the inner and outer trial functions of the two-zone approximation, respectively.

As the released fraction increases, one can calculate the locus of ρ at which the concentration is equal to 0.95 times its maximum by using Eqs. (2) and (3), which is designated as ρ_{drop}. As shown in Fig. 5, ρ_{drop} seems to be almost linear with respect to the fractional release. The distribution of the gas concentration is represented well if ρ_{drop} is assigned as ρ_2, and updated with the fractional release during the calculations. However, the relationship in Fig. 5 is neither applicable to the time-varying problem nor known in advance. It is

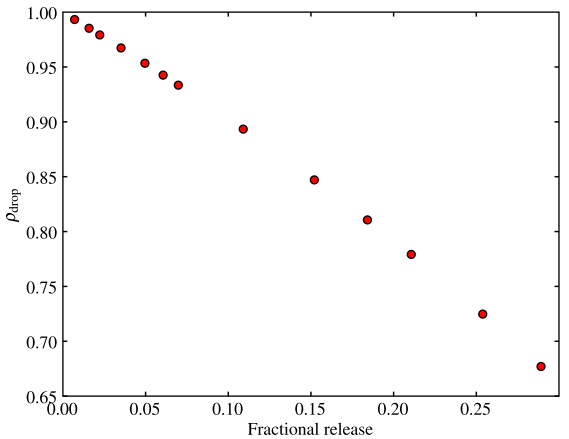

Fig. 5. The locus of the radial point as a function of the released fraction at which the concentration is equal to 0.95 times its maximum.

assumed that ρ_2 is updated by the linear equation as follows:

$$\rho_2(t) = 1 - \kappa_d \cdot f(t), \tag{4}$$

where f is the fractional release, and κ_d is a factor in the range of 0.5–1.05 which controls the update of ρ_2. The quadratic trial functions, C_1 and C_2 are a function of ρ_2 which varies during the calculations. The lower limit of ρ_2 is 0.8. ρ_3 is the midpoint of ρ_2 and 1, and ρ_1 is fixed at 0.4. In this way only ρ_2 is an independent variable.

C_1 and C_2 are derived by applying the boundary conditions at $\rho = 0$ and $\rho = 1$, and a continuity of the gas concentration at ρ_2. The trial functions are as follows:

For the inner region,

$$C_1(\rho) = \frac{25(\rho_2^2 - \rho^2)}{25\rho_2^2 - 4} c_1 + \frac{25\rho^2 - 4}{25\rho_2^2 - 4} c_2, \tag{5}$$

and for the outer region,

$$C_2(\rho) = \frac{(\rho - 1)(2\rho - \rho_2 - 1)}{(\rho_2 - 1)^2} c_2 + \frac{4(\rho - 1)(\rho_2 - \rho)}{(\rho_2 - 1)^2} c_3. \tag{6}$$

3.2. Stiffness matrix and load vector

The gas concentration c_g^0 at a time t becomes c_g after an increment of time δt. After integrating the diffusion equation for δt by using the backward Euler method, the variational form is derived by taking the product of the time-integrated diffusion equation with a trial function and integrating it over the domain. This gives

$$\delta \int_0^a 4\pi \left[\frac{D_{\text{eff}}}{2} \left(\frac{dc_g}{dr} \right)^2 + \frac{c_g^2}{2\delta t} - \left(\frac{c_g^0}{\delta t} + \beta \right) c_g \right] r^2 \, dr = 0. \tag{7}$$

Inserting the trial functions into Eq. (7) and minimizing the integral with respect to c_1, c_2, and c_3, leads to a set of equations,

$$\mathbf{K}\mathbf{c}_\mathbf{g} = \mathbf{b}, \tag{8}$$

where $\mathbf{K}$ represents the global stiffness matrix, $\mathbf{c}_\mathbf{g}$ the concentration vector, and $\mathbf{b}$ the load vector. $\mathbf{K}$ and $\mathbf{b}$ are the function of ρ_2.

Non-zero elements of the symmetric matrix $\mathbf{K}$ are given by

$$\begin{aligned}
K_{11} &= \frac{50A_8}{W_1^2}\frac{D_{\text{eff}}}{a^2} + \frac{10A_8A_9}{21W_1^2}\frac{1}{\delta t}, \\
K_{12} &= -\frac{50A_8}{W_1^2}\frac{D_{\text{eff}}}{a^2} + \frac{A_1A_8}{21W_1^2}\frac{1}{\delta t}, \\
K_{22} &= \frac{A_2}{15W_1^2W_2}\frac{D_{\text{eff}}}{a^2} + \frac{A_3}{210W_1^2}\frac{1}{\delta t}, \\
K_{23} &= -\frac{2A_4}{15W_2}\frac{D_{\text{eff}}}{a^2} + \frac{A_5W_2}{105}\frac{1}{\delta t}, \\
K_{33} &= \frac{16A_6}{15W_2}\frac{D_{\text{eff}}}{a^2} + \frac{8A_7W_2}{105}\frac{1}{\delta t},
\end{aligned} \tag{9}$$

where W_is and A_is are defined in Appendix A.

The last term in the integrand of Eq. (7) contains the product of c_g and c_g^0, which affects only $\mathbf{b}$. The interval of the integral needs to be adjusted as follows:

if $\rho_2 \leqslant \rho_{20}$,

$$\begin{aligned}
\int_0^1 c_g c_g^0 \, d\rho &= \int_0^{\rho_2} C_1 C_1^0 \, d\rho + \int_{\rho_2}^{\rho_{20}} C_2 C_1^0 \, d\rho \\
&\quad + \int_{\rho_{20}}^1 C_2 C_2^0 \, d\rho \\
&= \int_0^{\rho_2} C_1 C_1^0 \, d\rho + \int_{\rho_2}^1 C_2 C_2^0 \, d\rho \\
&\quad + \int_{\rho_2}^{\rho_{20}} C_2 (C_1^0 - C_2^0) \, d\rho,
\end{aligned} \tag{10}$$

otherwise,

$$\begin{aligned}
\int_0^1 c_g c_g^0 \, d\rho &= \int_0^{\rho_{20}} C_1 C_1^0 \, d\rho + \int_{\rho_{20}}^{\rho_2} C_1 C_2^0 \, d\rho \\
&\quad + \int_{\rho_2}^1 C_2 C_2^0 \, d\rho \\
&= \int_0^{\rho_2} C_1 C_1^0 \, d\rho + \int_{\rho_2}^1 C_2 C_2^0 \, d\rho \\
&\quad + \int_{\rho_2}^{\rho_{20}} C_1 (C_1^0 - C_2^0) \, d\rho,
\end{aligned} \tag{11}$$

where ρ_{20} is the interface coordinate at a time t.

Thus $\mathbf{b}$ has two cases depending on the magnitude of ρ_2 relative to ρ_{20}. In the range of ρ_2 to ρ_{20}, however, the difference between C_1 and C_2 is so small that only Eq. (10) is employed to calculate the integral irrespective of the sign of $\rho_2 - \rho_{20}$.

The elements of $\mathbf{b}$, b_i are arranged in a simplified form as a function of $\rho_{20} - \rho_2$,

$$b_i = \frac{1}{\check{b}_i} \sum_{j=0}^{m} \hat{b}_{i,j} (\rho_{20} - \rho_2)^j, \tag{12}$$

where $\check{b}_i$ and $\hat{b}_{i,j}$ are the denominator and the coefficient of the numerator, respectively. $\check{b}_i$s are given by

$$\begin{aligned}\check{b}_1 &= 21\delta t W_1 W_{10}/A_8,\\ \check{b}_2 &= 420\delta t W_1 W_{10},\\ \check{b}_3 &= 105\delta t W_{10}.\end{aligned} \tag{13}$$

In addition, **b** can be simplified further. Although m is in the range of the third to the ninth order, the contribution from the terms higher than the first order in Eq. (12) is negligible due to the small value of $\rho_2 - \rho_{20}$. Thus Eq. (12) is approximated by

$$b_i \approx (\hat{b}_{i,0} + \hat{b}_{i,1}(\rho_{20} - \rho_2))/\check{b}_i, \tag{14}$$

where $\hat{b}_{i,0}$ and $\hat{b}_{i,1}$ are summarized in Table 1, and Y_is are given in Appendix A.

3.3. Solutions of the system

In Eq. (9), let $K_1 = K_{11}$, $K_2 = K_{12}$, $K_3 = K_{22}$, $K_4 = K_{23}$, and $K_5 = K_{33}$.

The solution of the system of Eq. (8) is obtained simply by

$$\begin{aligned}c_1 &= (b_1K_4^2 - b_3K_2K_4 + (b_2K_2 - b_1K_3)K_5)/|\mathbf{K}_{3D}|,\\ c_2 &= (b_1K_2K_5 + K_1(b_3K_4 - b_2K_5))/|\mathbf{K}_{3D}|,\\ c_3 &= (b_3K_2^2 - b_1K_4K_2 + K_1(b_2K_4 - b_3K_3))/|\mathbf{K}_{3D}|,\end{aligned} \tag{15}$$

where $|\mathbf{K}_{3D}| = K_5K_2^2 + K_1(K_4^2 - K_3K_5)$.

The average gas concentration, $\bar{c}_g$ is given by

$$\bar{c}_g = \frac{A_8}{W_1}c_1 + \frac{Y_1}{20W_1}c_2 + \frac{W_2Y_6}{5}c_3. \tag{16}$$

In case of $\rho_2 = 0.8$, **K**, **b**, and $\bar{c}_g$ are reduced to those obtained by Matthews and Wood [4].

If the three DOFs are used fully during a whole stage, spurious fluctuations occur as shown in Fig. 4. Avoiding such an unacceptable profile is crucial in achieving a precise released fraction. This phenomenon can be written mathematically: the apex of C_2, ρ_{2v} is larger than ρ_2, or c_1 is less than c_2. In order to ensure that the gas concentration decreases monotonically, the number of DOF of Eq. (8) is reduced by the following criteria: $\partial C_2/\partial\rho = 0$ at ρ_2 if ρ_{2v} is larger than ρ_2 or if c_1 is less than c_2. Here the condition $\partial C_2/\partial\rho = 0$ leads to

$$\rho_{2v} = \frac{c_2(3+\rho_2) - 4c_3(1+\rho_2)}{4(c_2 - 2c_3)}. \tag{17}$$

In either case the DOF decreases from three to two. The condition of $\partial C_2/\partial\rho = 0$ at ρ_2 results in $c_3 = 3c_2/4$. Furthermore, if the system having the reduced DOF of 2 gives a solution such that c_1 is less than c_2 once again, c_1 is set to be equal to c_2. Thus the degree of freedom becomes one. Fig. 6 summarizes these criteria by which the solution of the system is determined during the calculations.

When DOF = 2, the concentrations at the nodal points are given by

$$\begin{aligned}c_1 &= (-16b_2K_2 - 12b_3K_2 + 16b_1K_3 + 24b_1K_4 + 9b_1K_5)/|\mathbf{K}_{2D}|,\\ c_2 &= 4((4b_2 + 3b_3)K_1 - 4b_1K_2)/|\mathbf{K}_{2D}|,\\ c_3 &= 3c_2/4,\end{aligned} \tag{18}$$

where $|\mathbf{K}_{2D}| = K_1(16K_3 + 24K_4 + 9K_5) - 16K_2^2$. When DOF = 1, the concentrations at the nodal points are given by

$$\begin{aligned}c_1 &= c_2,\\ c_2 &= 4(4b_1 + 4b_2 + 3b_3)/|\mathbf{K}_{1D}|,\\ c_3 &= 3c_2/4,\end{aligned} \tag{19}$$

where $|\mathbf{K}_{1D}| = 16K_1 + 32K_2 + 16K_3 + 24K_4 + 9K_5$. For both cases with the reduced DOF, Eq. (16) is also valid for $\bar{c}_g$.

3.4. Convergence criterion and automatic time integration

In the adaptive two-zone method, **K** and **b** are a function of ρ_2 which in turn is updated depending on the released fraction f. At every time step, several iterations are required to satisfy a convergence criterion of f which is given by

$$\varepsilon_i = \frac{f^{(p)} - f^{(p-1)}}{f^{(p-1)}}, \tag{20}$$

where the superscript p represents the p'th iteration. If a convergence is not reached within a given number of iterations, a solution is sought again with a reduced time increment.

Table 1
Coefficients of the numerators of the load vector

	$\hat{b}_{i,j} = \zeta\cdot\beta\delta t + \xi_1\cdot c_{10} + \xi_2\cdot c_{20} + \xi_3\cdot c_{30}$			
	ζ	ξ_1	ξ_2	ξ_3
$\hat{b}_{1,0}$	$7W_1$	$10A_9$	A_1	0
$\hat{b}_{1,1}$	Y_8	Y_8	0	0
$\hat{b}_{2,0}$	$7W_1Y_1$	$20A_1A_8$	$2A_3$	$4A_5W_1^2W_2$
$\hat{b}_{2,1}$	Y_1Y_8	$70A_9^2Y_7$	$2W_1Y_2$	$-8W_1\ Y_3$
$\hat{b}_{3,0}$	$7W_1W_2Y_6$	0	$A_5W_1W_2$	$8A_7W_1\ W_2$
$\hat{b}_{3,1}$	$W_2Y_6Y_8$	0	Y_4	$-4Y_5$

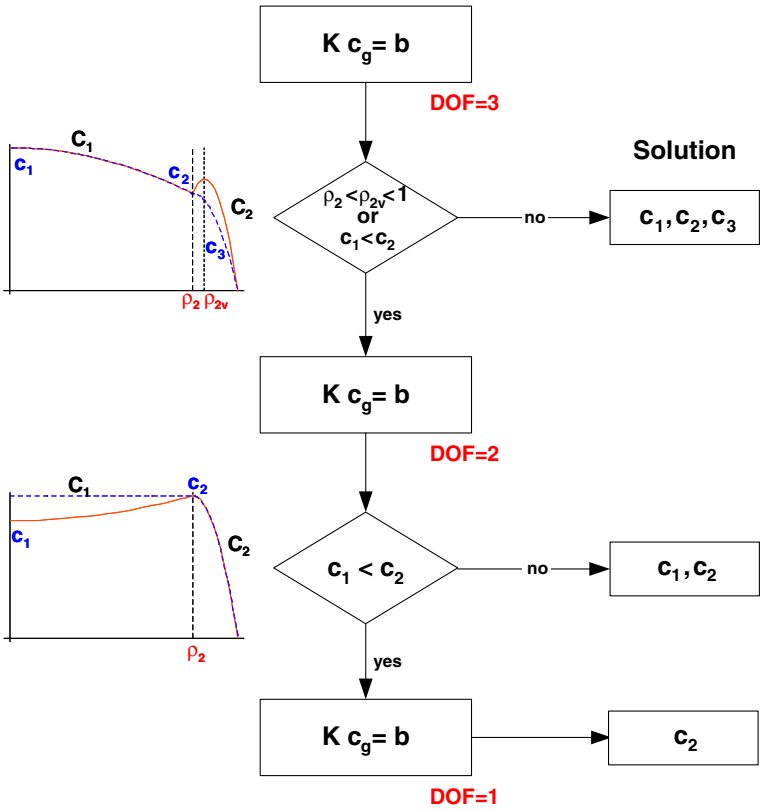

Fig. 6. Flowchart describing how DOF of the problem are determined.

To obtain a more efficient solution from the present method, an automatic time-integration method is employed. The time increment of the next time step Δt_{n+1} is predicted by comparing the fractional release between the consecutive time steps as defined by

$$R_f = \frac{|f(t_n) - f(t_{n-1})|}{f(t_{n-1})}. \tag{21}$$

Depending on the magnitude of R_f, Δt_{n+1} is automatically updated by the criteria

$$\Delta t_{n+1} = \begin{cases} 0.5\Delta t_n & \text{if } 0.1 < R_f, \\ \Delta t_n & \text{if } 0.1\gamma < R_f \leqslant 0.1, \\ 2\Delta t_n & \text{if } R_f \leqslant 0.1\gamma, \end{cases} \tag{22}$$

where γ is a factor controlling the update of the time increment.

In a reference calculation, the computational time of the adaptive two-zone method is compared with that of the algorithm by Forsberg and Massih [19,20] which is known for its superiority in the sense of an accuracy and efficiency. It is designated as the Forsberg–Massih algorithm. Compared to the Forsberg–Massih algorithm, the present method takes more computational time by about 40%. The computational time is measured by the total CPU time excluding input and output operations under the fixed time increment. Adopting the automatic time integration given in Eq. (22) makes it possible to reduce it substantially without a noticeable loss of the accuracy of the solutions.

4. Verification of the adaptive two-zone method

The validity of the proposed method is examined by comparing the fractional release with the reference solutions for a number of temperature and gas generation conditions. The fission rate is assumed to be linearly proportional to the temperature. The result of the ANS-5.4 algorithm is mainly used as the exact solution. To confirm the soundness of the present method as a numerical algorithm, the FEM solution with 50 quadratic elements is also obtained for every calculation.

The expression for the diffusion coefficient of the gas atoms is given in Table 2 [8]. The grain radius of 5 μm is used in the calculations.

Table 2
Diffusion coefficient used in the calculations [8]

Expression	$D_0 + D_1\exp(-Q_1/kT) + D_2\exp(-Q_2/kT)$
D_0	2.04×10^{-21} m^2/s
D_1	2.1×10^{-7} m^2/s
D_2	2.31×10^{-15} m^2/s
Q_1	3.85 eV
Q_2	1.37 eV

Fig. 7 shows an example of the responses of the gas released fraction as a function of the time. The temperature is fixed at 1200 °C.

The results from the reference FEM and the present method lie very close to the solution from the Booth approximation [2]. In the range of the fraction release less than 0.1, both numerical methods overestimate it by 10% or so. Although the error in this lower range depends more or less on how the time integration is performed, it is comparable to the other numerical methods [6,15,20]. The relative error becomes less than 1% at the end of the calculation.

At a very low time, for example, 1000 s, the released fraction is calculated to be 0.0036, 0.0051, and 0.0048 from the Booth approximation, the reference FEM, and the adaptive two-zone method, respectively. In view that the Forsberg–Massih algo-

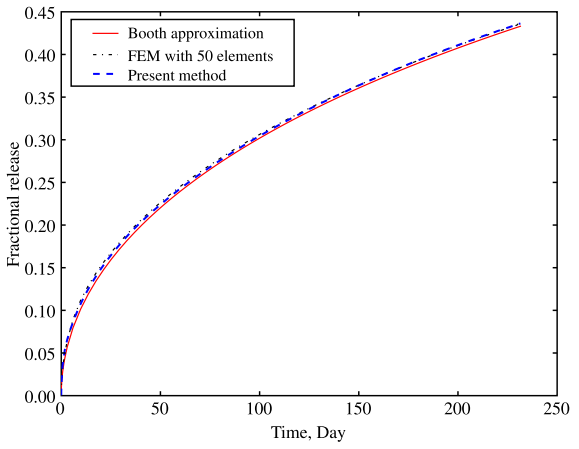

Fig. 7. Calculated fractional gas release as a function of the time at 1200 °C.

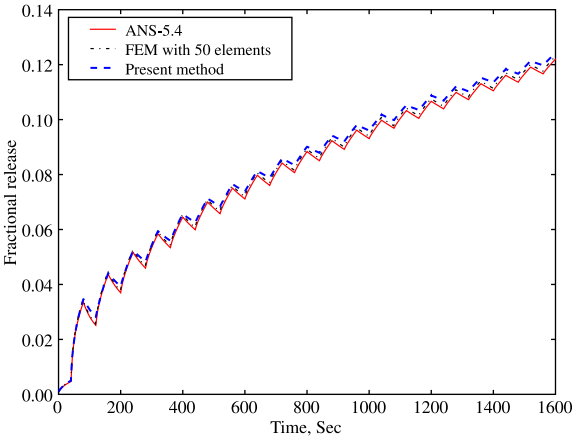

Fig. 8. Calculated fractional gas release as a function of the time for varying gas generation.

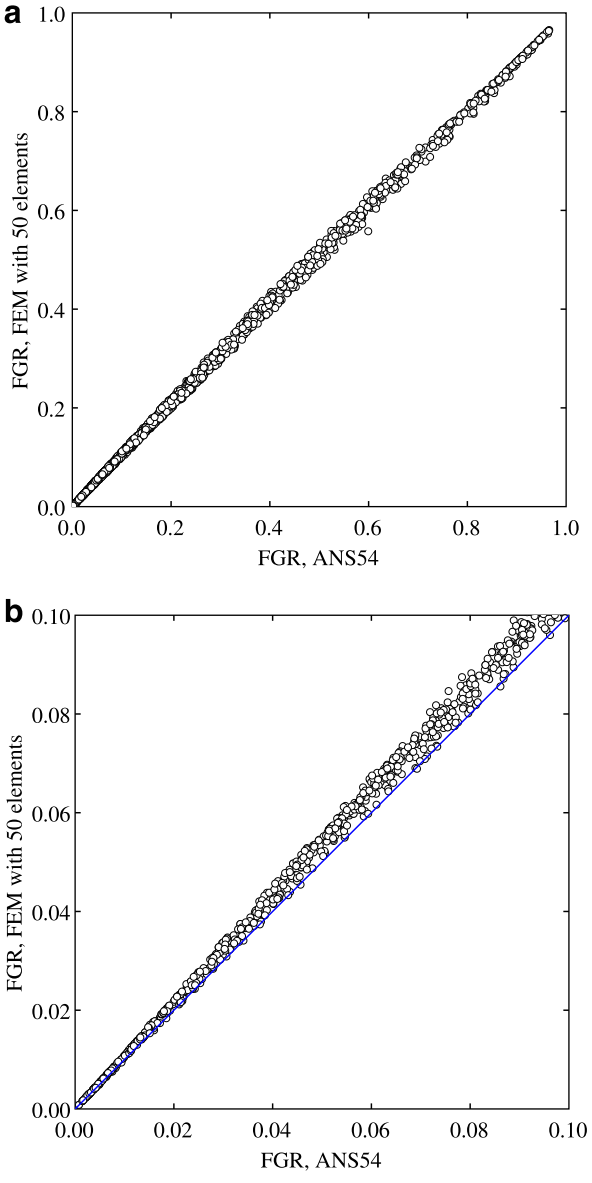

Fig. 9. FEM with 50 elements versus ANS-5.4 algorithm. (a) Whole range and (b) low release range.

rithm, whose accuracy was recently enhanced, has a maximum absolute error of 0.0014 [20], the present method yields quite an acceptable solution in the very low released fraction.

Fig. 8 shows the calculated fractional gas release as a function of the time when the temperature is subjected to changes as shown in Fig. 2. The present method gives a response very close to the reference solutions even though it is overestimated slightly during a temperature decrease and at the later stages.

By applying the methodology proposed by Lassmann and Benk [6], the present method has been extensively verified. For 2000 individual power histories which were randomly generated, the fractional release is compared with the solution from the ANS-5.4 algorithm. Each power history consists of 2–7 power stages during which the temperature is assumed to be constant in the range of 550–1550 °C. The number of the verification cases versus the fraction release follows a normal distribution with the mean of zero, where the cases in which the

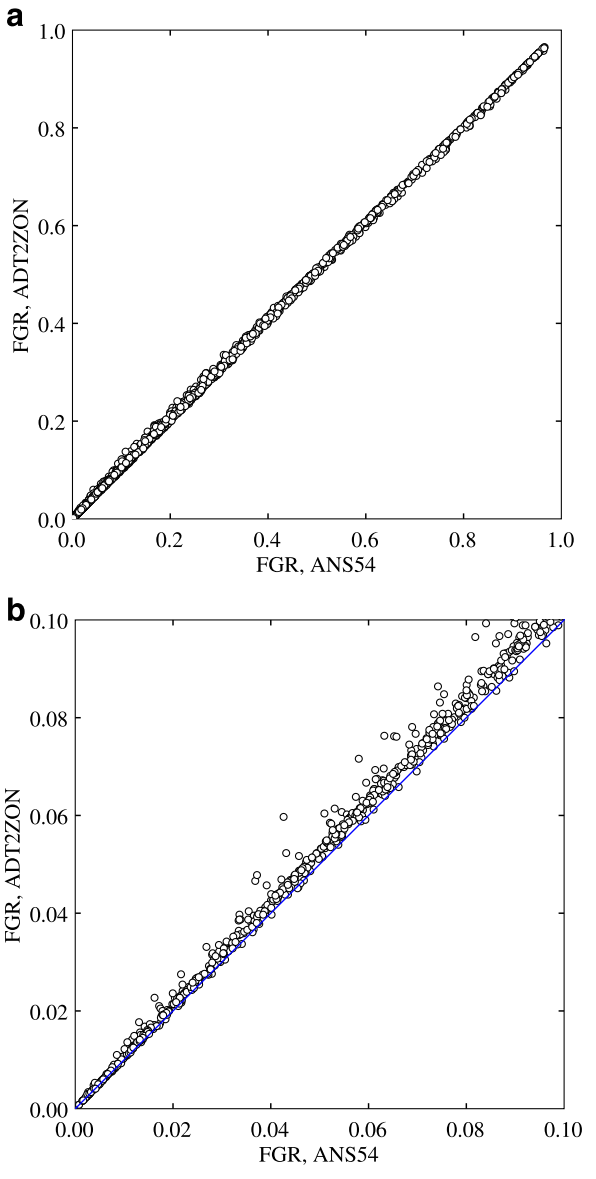

Fig. 10. Present method versus ANS-5.4 algorithm. (a) Whole range and (b) low release range.

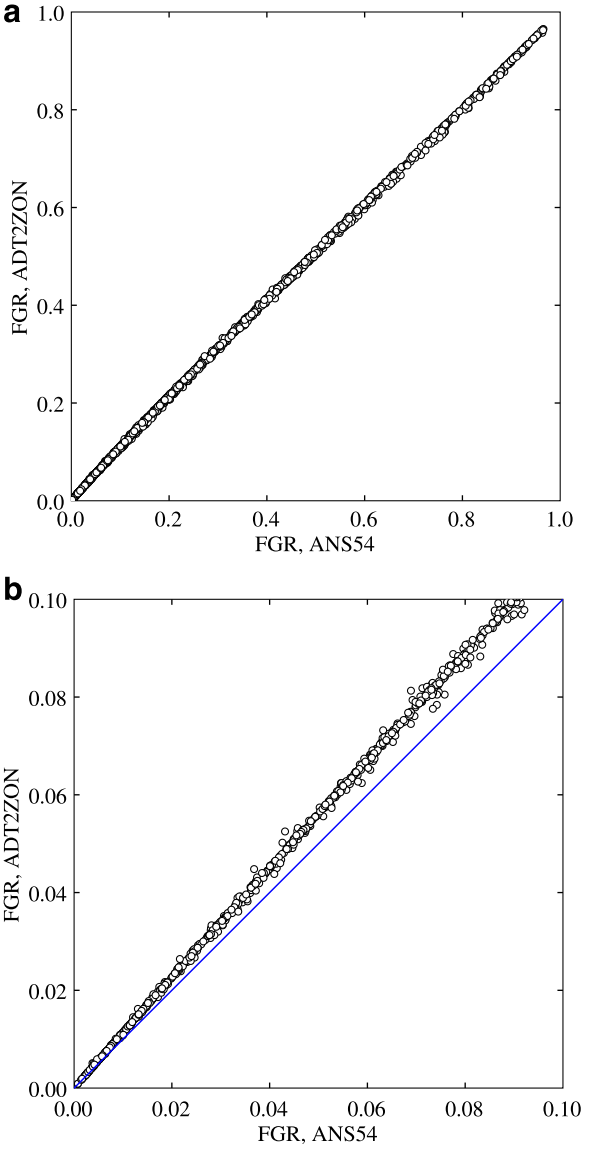

Fig. 11. Present method versus ANS-5.4 algorithm under a different moving strategy for ρ_2. (a) Whole range and (b) low release range.

released fraction is less than 0.3 are dealt with in more detail.

Fig. 9 shows the results from the reference FEM with 50 quadratic elements. For a comparison, those from the adaptive two-zone method are presented in Fig. 10. There exist some variations around the 45° line with a minor over-prediction in the lower range for both methods. The present method provides results equivalent to the reference FE calculation, even though there are a few cases showing a higher deviation. This is caused by an inappropriate relocation of ρ_2 during a lower temperature following a stage at which the temperature is rather high, and the fractional release in the lower range is less than 0.2.

The scattering around the 45° line shown in Fig. 10 is affected by what is chosen as κ_d in Eq. (4) for an updated ρ_2. Fig. 10 is generated by taking κ_d equal to 1.05. If $\kappa_d = 0.5$, the overall predictability seems to be improved in the whole range. In the lower range as shown in Fig. 11, meanwhile, the average of the predicted values lies a bit higher than the 45° line when compared to $\kappa_d = 1.05$.

The analysis above proves that the adaptive two-zone method is successfully applied to obtain the solution of the diffusion equation. The present method could be extended to treat numerically coupled equations in order to describe more complex behaviors at the grain boundaries, for example, to model the diffusion of gas atoms in the presence of an irradiation-induced resolution from a grain boundary.

5. Conclusion

An adaptive variational method has been developed to solve the diffusion equation for a fission gas release effectively and accurately. This approach is even more precise than the conventional two-zone method by Matthews and Wood, especially for a lower gas release. The present method could be easily applied to the situations with a non-zero gas concentration at the grain boundary.

Acknowledgements

The Ministry of Science and Technology (MOST) of the Republic of Korea has sponsored this work through the Mid- and Long-term nuclear R&D Project.

Appendix A

The coefficients W_i, A_i, and Y_i for the stiffness matrix and the load vector in Eq. (8) are given by

$$W_1 = 25\rho_2^2 - 4,$$
$$W_{10} = 25\rho_{20}^2 - 4,$$
$$W_2 = 1 - \rho_2,$$
$$A_1 = 75\rho_2^2 - 28,$$
$$A_2 = 6875\rho_2^6 + 13\,125\rho_2^5 - 2725\rho_2^4 - 1800\rho_2^3 - 232\rho_2^2 + 144\rho_2 + 48,$$
$$A_3 = 5000\rho_2^7 + 10\,625\rho_2^6 - 1500\rho_2^5 - 2775\rho_2^4 - 32\rho_2^3 + 72\rho_2^2 + 64\rho_2 + 16,$$
$$A_4 = 13\rho_2^2 + 4\rho_2 + 3,$$
$$A_5 = 6\rho_2^2 + 2\rho_2 - 1,$$
$$A_6 = 2\rho_2^2 + \rho_2 + 2,$$
$$A_7 = 2\rho_2^2 + 3\rho_2 + 2,$$
$$A_8 = 10\rho_2^5,$$
$$A_9 = 10\rho_2^2,$$
$$Y_1 = 75\rho_2^5 + 175\rho_2^4 + 31\rho_2^3 - 53\rho_2^2 - 12\rho_2 + 4,$$
$$Y_2 = 700\rho_2^4 + 1275\rho_2^3 - 38\rho_2^2 - 18\rho_2 - 8,$$
$$Y_3 = 700\rho_2^4 + 25\rho_2^3 - 138\rho_2^2 + 5\rho_2 - 4,$$
$$Y_4 = 350\rho_2^4 + 650\rho_2^3 + 171\rho_2^2 - 122\rho_2 - 20,$$
$$Y_5 = 350\rho_2^4 + 150\rho_2^3 - 149\rho_2^2 - 208\rho_2 + 4,$$
$$Y_6 = 3\rho_2^2 + 4\rho_2 + 3,$$
$$Y_7 = 15\rho_2^2 - 4,$$
$$Y_8 = 350\rho_2.$$

References

[1] Y.-H. Koo, B.-H. Lee, D.-S. Sohn, J. Kor. Nucl. Soc. 30 (1998) 541.
[2] A.H. Booth, A method of calculating fission gas diffusion from UO_2 fuel and its application to the X-2-f loop test, CRDC-721, 1957.
[3] W. Rausch, F. Panisco, ANS54: A computer subroutine for predicting fission gas release, NUREG/CR-1213, 1979.
[4] J.R. Matthews, M.H. Wood, Nucl. Eng. Des. 56 (1980) 439.
[5] C.S. Rim, Background and derivation of ANS-5.4 standard fission product release model, NUREG/CR-2507, 1982.
[6] K. Lassmann, H. Benk, J. Nucl. Mater. 280 (2000) 127.
[7] J. Turnbull, An assessment of fission gas release and the effect of microstructure at high burn-up, OECD Halden Reactor Project HWR-604, 1999.

[8] D.M. Dowling, R.J. White, M.O. Tucker, J. Nucl. Mater. 110 (1982) 37.
[9] K. Ito, R. Iwasaki, Y. Iwano, J. Nucl. Sci. Technol. 22 (1985) 129.
[10] P.V. Uffelen, Contribution to the modelling of fission gas release in light water reactor fuel, PhD thesis, Université de Liège, 2002.
[11] J. Rest, J. Nucl. Mater. 321 (2003) 305.
[12] T. Belytschko, W.K. Liu, B. Moran, Nonlinear Finite Elements for Continua and Structures, John Wiley & Sons, 2000.
[13] S. Roels, J. Carmeliet, H. Hens, Int. J. Numer. Methods Eng. 46 (1999) 1001.
[14] H.S. Carslaw, J.C. Jaeger, Conduction of Heat in Solids, Oxford University, USA, 1986.
[15] R.J. White, Fission gas release, OECD Halden Reactor Project HWR-632, 2000.
[16] ABAQUS, ABAQUS Analysis User's Manual, Version 6.5, 2004.
[17] J.-S. Cheon, Y.-H. Koo, B.-H. Lee, J.-Y. Oh, D.-S. Sohn, An adaptive two-zone method for numerical calculation of fission gas release, KAERI/TR-3183/2006, 2006.
[18] P.M. Gresho, R.L. Lee, Comput. Fluids 9 (1981) 223.
[19] K. Forsberg, A.R. Massih, J. Nucl. Mater. 127 (1985) 141.
[20] P. Hermansson, A.R. Massih, J. Nucl. Mater. 304 (2002) 204.